6th International Conference on Hydroinformatics - Liong, Phoon & Babovic (eds)

HYDRODYNAMIC FLOODPLAIN MODELING BASED ON HIGH-RESOLUTION LIDAR MEASUREMENTS

SEBASTIAN RATH
Department of River and Coastal Engineering, Technical University Hamburg
Denickestr. 22, 21073 Hamburg, Germany

ERIK PASCHE
Department of River and Coastal Engineering, Technical University Hamburg
Denickestr. 22, 21073 Hamburg, Germany

A concept to automate mesh generation for hydrodynamic finite element simulations is presented within a general framework for quality assessment, facing challenges for floodplain modeling based on high-resolution LiDAR measurements.

INTRODUCTION

Exploiting high-resolution measurements from Laser induced Detection and Ranging (LiDAR) for floodplain modeling is a current challenge for research in hydrodynamics. This challenge aims to improve efficiency in finite element mesh generation and consistency of simulations results. This concept reduces huge LiDAR data sets based on slope classification, routinely deriving case specific, adaptive surface meshes for hydrodynamic simulations and provides a mean for fast data exploitation. Applications of computational fluid dynamics commonly recognize, that mesh resolution is the only unbounded parameter value where specific boundaries and error bands have not yet been considered up to now [8]. Providing this model concept seeks stimulation for further efforts in that particular field of hydrodynamic mesh generation.

ACCURACY OF FLOODPLAIN MODELING BASED ON LIDAR DATA

Accuracy standards for LiDAR data, given by the US Federal Emergency Management Agency (FEMA) for floodplain mapping in accordance with the US National Standard for Spatial Data Accuracy (NSSDA) for digital products, claim that an accurate DEM should have a maximum Root Mean Square Error (RMSE) of 15 cm [7]. The RMSE is the square root of the average of a set of squared differences between LiDAR coordinate values and coordinate values from an independent source of higher accuracy for identical points. Moreover, 95 percent of any sufficiently large sample should be less than 1.96 times the RMSE, holding for normally distributed differences averaging zero. Thus, a RMSE of 15 cm is referred to as '30-centimeter accuracy at the 95-percent confidence level'. The vertical accuracy of any DEM is defined as 1.96 times the RMSE of linearly interpolated elevations in the DEM. Mean values exceeding ± 2 cm or values of the coefficient of skew outside ± 0.5 cm may indicate systematic errors. Contractors must test a least 20 test points for each major vegetation category and to show they accomplish

$$RMSE_{sample} \leq 15\sqrt{\frac{(n-1)-2.326\sqrt{n-1}}{n}} \quad (1)$$

where n is the number of test points in the sample and $RMSE_{sample}$ is determined in cm-units. Random errors magnitudes in LiDAR data accomplish ± 20 cm on flat paved terrains, increasing to ± 200 cm on hilly terrain with grass and scrubs [10].

MODEL CONCEPT

This model concept handles entire high-resolution data sets, e.g. riverbeds and floodplains. Realized as modular system it currently finds its first applications, aiming to determine bounds for hydrodynamic mesh generation. It supplies local adaptive mesh density while representing important structures and holding geometric requirements for finite element simulations.

MODEL APPROACH

The most effective terrain discretization uses the less points of the original data set for a finite element mesh, provides suitable numerical performance and appropriate simulation results. This ultimate representation cannot be found a priori, but is assessable by gradual abstraction or refinement of the initial mesh and revision of their inductive manipulation on the hydrodynamics via this model concept. A models value should be evaluated via its capacity to reproduce outflow hydrographs, flood extents, water depths and velocities. A models accuracy reflects upon the accumulation of weighted errors in the discretization of the physical terrain, its roughness inducing friction losses and turbulence. Focusing merely on terrain representation, this paper suggests an error bound E for the domain Ω, depending on the accuracy of the LiDAR data set, i.e. its RMSE, and the 'grade of abstraction for the representation'. The model concept uses a global, terrain specific scale of detail Δ for representation of terrain and its flow relevant features. This scale must avoid disparities, requiring compensation in the model calibration process. Numerical costs can be optimized via the local maximum tolerance factor α, representing important features within the bound of E, such that for each vertice of the finite element mesh

$$\mathrm{E}(\Omega) \leq RMSE + \alpha \cdot \Delta \quad (2)$$

where generally $\alpha = 1$, except for break line locations where $\alpha > 1$ if $\alpha > \Delta$. Random fractions of LiDAR data suite to determine the impact of $\alpha \cdot \Delta$. A Lower bound on residuals serves for local refinement and higher for direct inclusion of measurements to the TIN. The last strategy is sensitive towards random errors in LiDAR data. Both strategies increase the mesh density.

MODEL STRUCTURE

The model structure essentially consists of an initial surface grid, its classification into a breakpoint matrix and their concatenation to a set of polygonal break line vectors. The

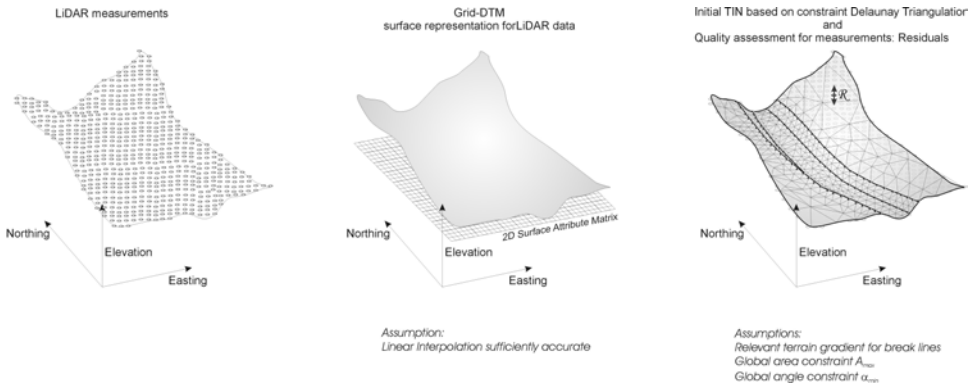

Figure 1. Gridding LiDAR data to derive break lines, being represented in a TIN.

last structure serves as boundary condition for a final surface mesh. Final surface meshes for hydrodynamics on floodplains are derived by a Delaunay refinement, i.e. the final mesh is an irregular triangular network (TIN). This model structure including break line representation is beyond similar notions for meshing scattered high-resolution bathymetric data sets based on B-Spline surfaces, representing topography based on a regular grid of de Boor points [2].

BREAKPOINT CLASSIFICATION

Recognizing terrain slope as governing factor for floodplain modeling, LiDAR data requires a surface representation for breakpoint localization. A high-resolution grid surface is considered as favorable choice, seeking simplicity in data ruling for the concatenation of breakpoints to break lines. Figure 1 shows that surface attributes are reflected as 2D matrices in the grid representation. The terrain specific scale of detail for breakpoint localization designates half the chosen grid resolution. Their vertical accuracy relates to the interpolation method during grid generation. Linear interpolation induces a vague surface smoothing and contributes to partly eliminate the inherent disparity in LiDAR measurements. Two alternate concepts are feasible to determine breakpoints for Grid-DTMs: 1st order derivative breakpoint localization, ‘slope methods’, and 2nd order derivative breakpoint localization, ‘change of slope methods’.

SLOPE METHODS

Slope methods express the first order derivative for the grid elevation matrix. A review of various assessed weighting concepts using a 3x3 kernel to determine slope in Grid-DTMs is given in Table 1. Applying a threshold for a critical slope $S_{crit.}$ on the floodplains, the boundaries of flow relevant structures or areas are extractable via a thinning procedure. A suitable thinning discards breakpoint being completely surrounded by other breakpoints (e.g. an interior point on a hill shade). Final achievement is a slope matrix and its thinned binary classification matrix.

Table 1. Feasible methods for slope assessment in Grid-DTMs.

	Method, *Authors*	Slope-Formulas	GIS-Appliance	Ref.
1st ORDER derivative: 'slope' based on 3x3 kernel definition: z_1 z_2 z_3 / z_8 z_9 z_4 / z_7 z_6 z_5	Max. Slope, *Shanholtz (1990)*	$S = \text{atan}\left(\max\left(\frac{\lvert z_9 - z_i \rvert}{L_c}\right)\right)\frac{180°}{\pi}$	IDRISI	[6]
	One-Over-Distance	$S = \text{atan}\left(\sqrt{S_{e-w}^2 + S_{n-s}^2}\right)\frac{180°}{\pi}$ $S_{e-w} = \frac{(z_3 + \sqrt{2}z_4 + z_5) - (z_1 + \sqrt{2}z_8 + z_7)}{(4 + 2\sqrt{2}) \times d}$ $S_{n-s} = \frac{(z_1 + \sqrt{2}z_2 + z_3) - (z_7 + \sqrt{2}z_6 + z_5)}{(4 + 2\sqrt{2}) \times d}$	NOAA	[11]
	Neighborhood, *Sharpnack & Akin (1969)*	$S = \text{atan}\left(\sqrt{S_{e-w}^2 + S_{n-s}^2}\right)\frac{180°}{\pi}$ $S_{e-w} = \frac{(z_3 + 2z_4 + z_5) - (z_1 + 2z_8 + z_7)}{8 \times d}$ $S_{n-s} = \frac{(z_1 + 2z_2 + z_3) - (z_7 + 2z_6 + z_5)}{8 \times d}$	ArcInfo, GRASS	[6] [17]
	Constraint-Quadratic, *Wood (1996)*	$S = \text{atan}\left(\sqrt{S_{e-w}^2 + S_{n-s}^2}\right)\frac{180°}{\pi}$ $S_{e-w} = \frac{(z_3 + z_4 + z_5) - (z_1 + z_8 + z_7)}{6 \times d}$ $S_{n-s} = \frac{(z_1 + z_2 + z_3) - (z_7 + z_6 + z_5)}{6 \times d}$	ERDAS Imagine	[11]
	Quadratic-Surface (Rook's Case), *Zenvenbergen & Thorne (1987)*	$S = \text{atan}\left(\sqrt{S_{e-w}^2 + S_{n-s}^2}\right)\frac{180°}{\pi}$ $S_{e-w} = \frac{z_4 - z_8}{2 \times d}$ $S_{n-s} = \frac{z_2 - z_6}{2 \times d}$	Surfer	[6] [13] [17]
	Diagonal-Ritter (Queen's case)	$S = \text{atan}\left(\sqrt{S_i^2 + S_j^2}\right)\frac{180°}{\pi}$ $S_i = \frac{z_5 - z_1}{2\sqrt{2} \times d}$ $S_j = \frac{z_3 - z_7}{2\sqrt{2} \times d}$		[11]
2nd ORDER derivative: 'change of slope'	Laplacian of Gaussian (LoG), *Marr & Hildreth (1980)*	$H(x,y) = \frac{1}{\pi\sigma^4}\left(1 - \frac{r}{2\sigma^2}\right)\exp\left\{\frac{r}{2\sigma^2}\right\}$		[12]

With the grids cell dimension d, the four directions e, w, n and s, the distance from z_9 to its neighboring grid cells L_c (either d or $\sqrt{2}d$) and the standard deviation σ relating to the size of the Gaussian kernel and $r=x^2+y^2$.

CHANGE OF SLOPE METHODS

Second order derivative edge detection focuses on intensity changes in image analysis or high-resolution grid terrain surveys. The use of the Laplacian to convolve the surface derives a corresponding zero–cross matrix, which determines edge locations in the

second derivative [9]. The edge Laplacian *G(x,y)* of a continuous, grid elevation matrix *F(x,y)* is defined by

$$G(x,y) = -\nabla^2 \{F(x,y)\} \tag{3}$$

with the Laplacian giving the sum of both second derivative spatial directions

$$\nabla^2 = \frac{\partial^2}{\partial x^2} + \frac{\partial^2}{\partial y^2} \tag{4}$$

Zero crossings of the edge Laplacian *G(x,y)* indicate the presence of edges. *G(x,y)* is zero if *F(x,y)* is constant or changing linearly in amplitude. If the rate of change is more than linear, *G(x,y)* exhibits a sign change at the point of inflection of *F(x,y)*. The negative sign in the definition of the edge Laplacian causes a positive slope for an edge whose amplitude increases from left to right or bottom to top within the grid. The general form of the convolution operation expresses Eq. (3) as

$$G(x,y) = F(x,y) * H(x,y) \tag{5}$$

Convolution masks *H* are sensitive to noise. Gaussian smoothing of *F(x,y)* before applying the Laplacian reduces high frequency noise components prior to differentiation and regularizes the derivative computation. This method is named the Laplacian of Gaussian (LoG). Its analytic expression of this operation is given in Table 1. *Pratt* gives the gain-normalized expression for a separable eight-neighbor notation [12]:

$$H = \frac{1}{8}\begin{bmatrix} -2 & 1 & -2 \\ 1 & 4 & 1 \\ -2 & 1 & -2 \end{bmatrix} \tag{6}$$

The LoG method provides a binary classification matrix based on a sensitivity threshold, analogous to the slope method. 2nd order edge detection suffers from the interpretation of the LoG-Response. Errors occur due to missing valid edge points, edge point localization failures and misclassification due to noisy raw data. A similar notion to detect VIP points was developed by *Chen et al.* [5].

COMPARISON

Local quality assessments sets indicate, that the LoG-method is less suitable weighted against the first order derivative slope methods. Its focus on intensity changes tends to access points referring to random errors in the LiDAR measurements. Its access to break lines can remain incomplete. So far experienced within this model concept, most appropriate breakpoint sets for further concatenation to break lines are derived with the One-Over-Distance method together with an appropriate terrain specific $S_{crit.}$ for thinning.

BREAKLINE DELINEATION

Automated delineation of break lines from depicted breakpoint matrices involves a framework of following conventions: Only breakpoints are connected. Concatenation

candidates are grid-neighboring breakpoints. Slope in between break line segments varies continuously and less than $S_{crit.}$

These conventions derive contiguous break lines, avoid interpretations due to gaps in break lines and prevent inclusions of unrealistic terrain steps. Following priority queue suites to derive breakpoint concatenations with a dynamic 3x3 kernel processing the breakpoint matrix: Breakpoints opening new break lines initialize *n* paths directed towards their *n* neighboring candidates. Except for breakpoints opening new break lines, breakpoints cannot be referred to more than one break line. Considering break line courses during concatenation, suitable candidates do not exceed its current trend for more than ± 90°. In shallow areas such as floodplains or deltas, the most appropriate candidate amongst others, fulfilling these priorities, returns the concatenation with the least slope, whereas in terrains with considerable terrain slope, the most appropriate candidate returns the least change of slope for its break line. Situations raising uncertain concatenation situations despite these priorities are overcome, enlarging the kernel to 7x7 cells, using stochastic determinations for break line evolution or strictly path-evolution related rules.

Line simplification requires the accuracy bound α. and is a worthwhile attempt reducing finite element mesh densities, applying purely statistical thinning, the Douglas-Peucker method or cubic polynomial splining, suggested by *Brüggelmann* [3].

DELAUNAY REFINEMENT

The model concept uses Delaunay refinements for adaptive hydrodynamic floodplain meshing and represents break line as Planar Straight Line Graphs (PSLGs), being a set of vertices and segments [15]. This conforming triangulation applies constraints while using the Delaunay criterion to govern the concatenations of the node set. It requires that the circumcircle of a triangle encloses no other vertex of the triangulation. Initializing a triangulation based on break lines and the domain boundary, additional Steiner points are introduced while meshing the floodplains to fulfill the constraints as well as the Delaunay criterion. A minimum-angle-bound prevents ill-conditioned equation systems within the finite element method [4] and implicitly prevents large angles, implying errors in the gradients of the interpolated surface [1]. A maximum-area-bound ensures local accuracy for the allocation of element-to-node-contributions by means of the weighting function. Both constraints are handled via Rupert's Refinement algorithm [14]. Steiner points elevations are available via interpolation from the grid elevation matrix. The model concept applies the open-source algorithm *Triangle*, developed by *Shewchuck* [16].

MODEL APPLICATION

Automatically meshing the river junction Bramau/Stoer in Northern Germany accesses a LiDAR data density of nine measurements per square meter. Breakpoint extraction is performed by the One-Over-Distance method on a 1m-grid. $S_{crit.}$=10° denotes the shallow terrain and derives suitable breakpoint sets at the scale of detail $\Delta = 0.5m$. Within a rectangular domain a Delaunay refinement based on thinned break lines description, a

100m²-maximum-area-bound of and a 25°-minimum-angle-bound is performed. Figure 2 illustrates thinned break lines, retaining simply every 4th breakpoint, denoting a maximum tolerance factor $\alpha = 1.8$. The grade of abstraction equals 0.9m for this mesh. The inverted map uses a random color shading to show that natural break lines are retrieved as multiple components, high lightning particularly brightly shaded break line components. Using 0.1% of the LiDAR data for quality assessment of this terrain representation yields dominantly residuals below 10cm (gray pixels). Less residuals amount to 10-25cm (white pixels). No residual exceeds 25cm. Hydrodynamic simulations for this terrain representation verify the applicability of this method.

CONCLUSION

This concept for automatic meshing provides a fast and efficient method to exploit high-resolution data. It generates various scales of terrain representation at predictable error bounds. Furthermore, the concept contributes a vital basis to assess the impact of mesh resolution in hydrodynamics and its impact on friction losses and turbulence modeling.

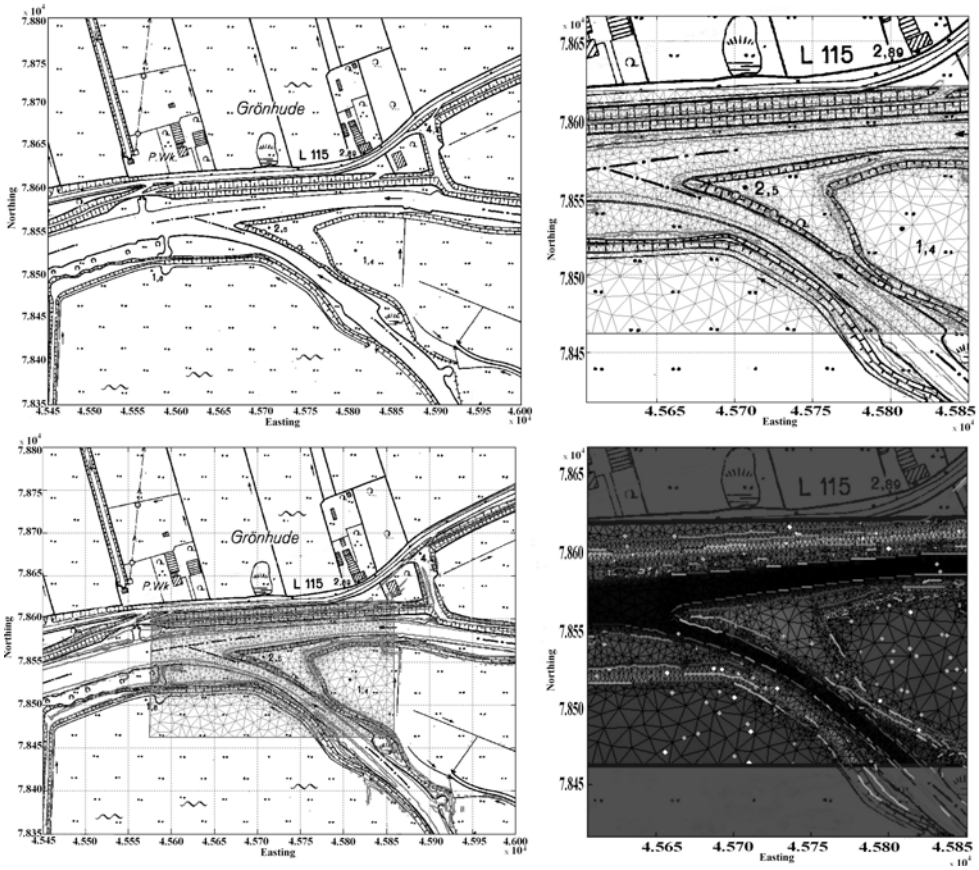

Figure 2. Automatically meshing the river junction Stoer/Bramau, Northern Germany.

REFERENCES

[1] Babuška I. and Aziz A.K., "On the angle condition in the finite element method", *SIAM Journal of Numerical Analysis*, Vol.13, No.2, (1976), pp 214-226.

[2] Berkhahn V., Göbel M., Stoschek O. and Matheja A., "Generation of adaptive finite element meshes based on approximation surfaces", *Proc. 5th Int. Conf. on Hydro-Science and –Engineering, (ICHE 2002), Warsaw, Poland*.

[3] Brügelmann R., "Automatic breakline detection from airborne range data", *Int. Arch. of Photogrammetry and Remote Sensing*, Vol. 33, Part B3, (2000), pp 109-116.

[4] Carey G.F. and Oden J.T., "*Finite Elements: Computational Aspects*", Prentice-Hall, (1984).

[5] Chen Z. T. and Guevara J.A., "Systematic selection of very important points (VIP) from digital terrain model for construction triangular irregular networks", Autocarto 8, Proceedings of the Society for Photogrammetry and Remote Sensing, (1987).

[6] Dunn M. and Hickey R., "The effect of slope estimates within GIS", *Cartography*, Vol. 27, No.1, (1998), pp 9-15.

[7] FEMA, "Accuracy specifications for LiDAR DEM for floodplain mapping", *Internet Service,* (2004), www.fema.gov/mit/tsd/mm_a4b7.shtm

[8] Hardy R.J., Bates P.D. and Anderson M.G., "The importance of spatial resolution in hydraulic models for floodplain environments", *Journal of Hydrology*, Vol. 216 (1999), pp 124-136.

[9] Huertas A., and Medioni G., "Detection of intensity changes with sub pixel accuracy using Laplacian-Gaussian masks*", IEEE Transactions on Pattern Analysis and Machine Intelligence*, Vol. 8, (1986), pp 651-664.

[10] Huising E.J. and Gomes Pereira L.M., "Errors and accuracy estimates of laser data acquired by various laser scanning systems for topographic applications", *ISPRS Journal of Photogrammetry & Remote Sensing*, Vol. 53 (1998), pp 2544-261.

[11] Jones K.H., "A comparison of algorithms used to compute hill slope as a property of the DEM", *Computers & Geoscience*, Vol. 24 (1998), pp 315-323.

[12] Pratt K.W., *"Digital Image Processing"*, John Wiley & Sons (1991), pp 698.

[13] Ritter P., "A vector-based slope and aspect generation algorithm", *Photogrammetric Engineering and Remote Sensing*, Vol. 53, No. 8, (1987), pp 1109-1111.

[14] Rupert J., "A Delaunay refinement algorithm for quality 2D-mesh generation", *Journal of Algorithms*, 18, No.3, (1995), pp 548-585.

[15] Shewchuck J.R., "Delaunay refinement algorithms for triangular mesh generation", *Computational Geometry: Theory and Applications*, Vol. 22 (1-3), pp 21-74, (2002).

[16] Shewchuck J.R., "Triangle: Engineering a 2D Quality Mesh Generator and Delaunay Triangulator", *Proc. 1st Workshop on Applied Computational Geometry*, Philadelphia, Pennsylvania, (1996), pp 124-133.

[17] Skidmore A., "A comparison of techniques for calculating gradient and aspect from a gridded digital elevation model", *International Journal of GIS*, Vol. 3, No. 4, (1989), pp 323-334.